Letters

A Truly NTD-Based PLL: Simple Approach of Double-Frequency Oscillation Rejection

Mohd. Afroz Akhtar, *Student Member, IEEE*, and Suman Saha

***Abstract*—Nonfrequency-dependent transport delay phase-locked loop (NTD-PLL) comprised of an additional transport-delay (TD) unit in the Park transformation matrix (TM), supposedly to improve the offset and double-frequency oscillatory errors (DFOEs) during the frequency deviations. This modification in the Park TM, however, does not eliminate the DFOEs from all the estimation parameters of the utility grid. It is shown in this letter that the issue can be completely alleviated from all the estimation parameters of the grid just by adding another TD unit in the Park TM of NTD-PLL. The effectiveness of the suggested approach is verified through numerical and experimental results.**

***Index Terms*—Linear time-periodic (LTP), phase-locked loop (PLL), synchronization, transformation matrix (TM), transport delay (TD).**

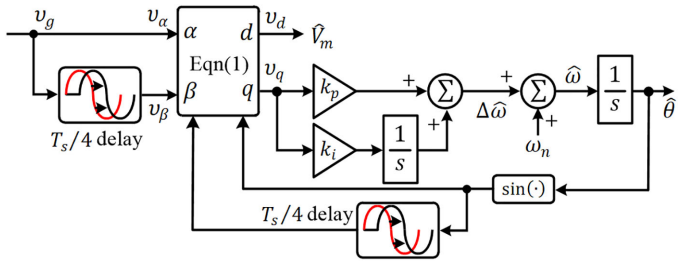

Fig. 1. Block diagram of basic NTD-PLL. v_g is the grid voltage. The terms $\hat{V}_m$, $\hat{\omega}$, and $\hat{\theta}$ are the estimated amplitude, angular frequency, and phase angle of v_g, respectively. ω_n is the nominal frequency, and k_p and k_i are the control parameters.

I. Introduction

ESTIMATION of the utility grid voltage parameters (i.e., phase, frequency, and amplitude) are crucial for synchronization, control, monitoring, and protection of grid-connected converters, which are often provided by using a phase-locked loop (PLL) technique [1]. Large numbers of PLLs for single-phase grid have been designed in recent years [2], [3]. A challenging problem to design a single-phase PLL is generating a fictitious quadrature signal, v_β, for its operation. From the various state-of-the-art algorithms used to generate quadrature signal viz-a-viz inverse Park transform [1], second-order generalized integrator [4], all-pass filter [5], and quarter-cycle transport delay (TD); the TD unit is a simple and popular approach [2], [3]. The TD-based PLL utilizes fixed quarter-cycle $T_s/4$ TD, where T_s is the time period of the fundamental component of the nominal grid frequency [3]. It means that the phase difference between in-phase and fictitious quadrature-phase signals may not be orthogonal (i.e., 90°) under frequency deviations, thus leading to offset and double-frequency oscillatory errors (DFOEs) [1]–[3] in the estimated quantities. The nonfrequency-dependent transport-delay-based PLL (NTD-PLL) [2], [3] which is the focus of the letter, is a simple and popular approach to deal with the challenge of TD-PLL. The NTD-PLL as shown in Fig. 1 introduces another $T_s/4$ delay in the transformation matrix (TM) to indirectly generate $\cos(\hat{\theta})$ from $\sin(\hat{\theta})$ for the Park TM [1], [2]. The TD-based Park TM, $R_{PT}(\hat{\theta})$ for the NTD-PLL is expressed in (1), wherein

$$\hat{\theta} = \int \hat{\omega} dt \; = \int (\omega_n + \Delta\hat{\omega})\, dt \; = \omega_n\, t + \int \Delta\hat{\omega} dt$$

$$R_{PT}\left(\hat{\theta}\right) = \begin{bmatrix} -\sin\left(\hat{\omega}\,(t - T_s/4)\right) & \sin\left(\hat{\omega} t\right) \\ -\sin\left(\hat{\omega} t\right) & -\sin\left(\hat{\omega}\,(t - T_s/4)\right) \end{bmatrix}$$

$$= \begin{bmatrix} \cos\left(\hat{\theta} - \Delta\hat{\omega}\,(T_s/4)\right) & \sin\left(\hat{\theta}\right) \\ -\sin\left(\hat{\theta}\right) & \cos\left(\hat{\theta} - \Delta\hat{\omega}\,(T_s/4)\right) \end{bmatrix} \tag{1}$$

and $\omega_n = 2\pi/T_s$ is the nominal grid frequency and $\Delta\hat{\omega}$ is the estimation of frequency deviation from its nominal value (both in rad/s), respectively. It is shown in [2] that the NTD-PLL can correct the phase-offset problem of basic TD-PLL during frequency jump, but it cannot solve the DFOEs in $\hat{\omega}$ and $\hat{\theta}$ estimation (see Fig. 20 of [2]). In yet another modified NTD-PLL (mNTD-PLL) [6], the TD-based Park TM is modified wherein the $\sin(\hat{\theta})$ is indirectly generated from $\cos(\hat{\theta})$. The TM $R_{mPT}(\hat{\theta})$ for the mNTD-PLL [6] is expressed as

Manuscript received June 24, 2021; revised August 1, 2021; accepted August 17, 2021. Date of publication August 27, 2021; date of current version October 15, 2021. *(Corresponding author: Mohd. Afroz Akhtar.)*

Mohd. Afroz Akhtar and Suman Saha are with the Academy of Scientific and Innovative Research, CSIR-CMERI Campus, Durgapur 713209, India, and also with the Aerosystems Laboratory, CSIR-Central Mechanical Engineering Research Institute, Durgapur 713209, India (e-mail: afrozakhtar@cmeri.res.in; s_saha@cmeri.res.in).

Color versions of one or more figures in this article are available at https://doi.org/10.1109/TPEL.2021.3107773.

Digital Object Identifier 10.1109/TPEL.2021.3107773

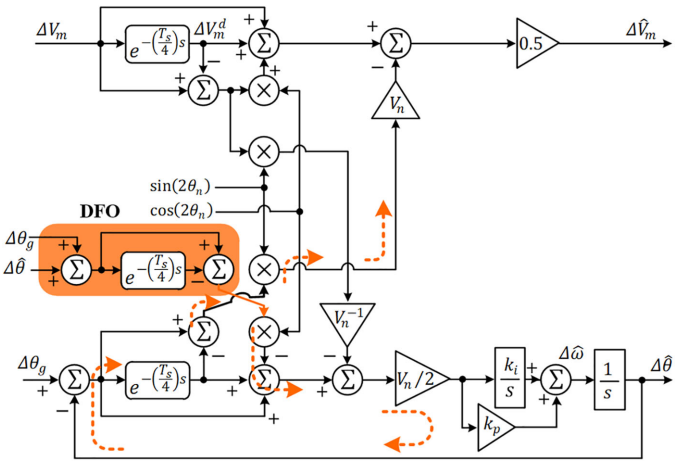

Fig. 2. LTP model of NTD-PLL.

$$R_{mPT}\left(\hat{\theta}\right) = \begin{bmatrix} \cos\left(\hat{\theta}\right) & \sin\left(\hat{\theta} - \Delta\hat{\omega}\,(T_s/4)\right) \\ -\sin\left(\hat{\theta} - \Delta\hat{\omega}\,(T_s/4)\right) & \cos\left(\hat{\theta}\right) \end{bmatrix}. \quad (2)$$

It is shown in [6] that compared to NTD-PLL, the mNTD-PLL reduces the offset error as well as DFOEs in $\hat{\omega}$ and $\hat{\theta}$ estimation to zero during frequency deviation. However, the $\hat{V}_m$ of the mNTD-PLL now suffers from DFOE under frequency drift. It is evident from [1], [2], [6] that the response one or more grid parameters estimated from NTD-PLL as well as mNTD-PLL are dependent on the frequency deviation which remains a challenge in the NTD-based PLL design.

In this letter, we are proposing a simple yet efficient NTD-PLL design, which is capable of eliminating the DFOEs from all the estimation parameters of the grid under the frequency deviation. To this end, the dynamic response of NTD-PLL and mNTD-PLL has been analyzed in a linear-time periodic (LTP) [7] framework. A truly NTD-PLL, concisely called the tNTD-PLL structure is proposed wherein the response of $\hat{\omega}$, $\widehat{\theta}$, as well as $\hat{V}_m$ estimations obtained from proposed structure are not dependent on frequency deviation. The suggested tNTD-PLL eliminates the DFOEs from the estimation parameters by modifying the TM while still inheriting the simplicity of the standard NTD-PLL, which, to the best of the authors' knowledge, has not been explored before.

II. Truly Nonfrequency-Dependent TD-PLL (tNTD-PLL)

Figs. 2 and 3 show the LTP structures of NTD-PLL and mNTD-PLL, respectively [6]. The propagation of the impact of the DFO term $(\Delta\theta_g + \Delta\hat{\theta}) - (\Delta\theta_g^d + \Delta\hat{\theta}^d)$ [6], mainly responsible for the DFOEs in the estimated parameters of the grid is also highlighted in Figs. 2 and 3. It is observed that the DFOE term is added in the control loop of the NTD-PLL, i.e., υ_q, thus leading to oscillatory error in $\hat{\theta}$ and $\hat{\omega}$. Further more, due to the cross-coupling between amplitude and phase estimation loops in the NTD-PLL, the amplitude estimation, $\hat{V}_m$ obtained from υ_d

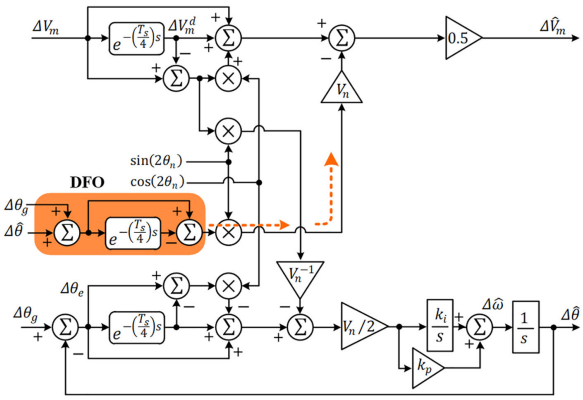

Fig. 3. LTP model of mNTD-PLL.

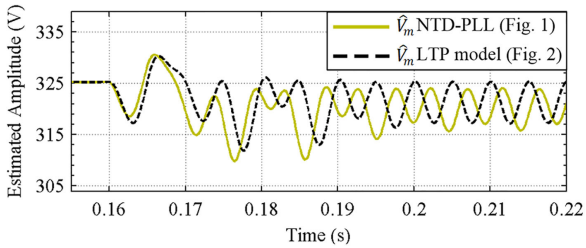

Fig. 4. Assessment of oscillations in $\hat{V}_m$ of NTD-PLL in presence of a +3 Hz frequency jump.

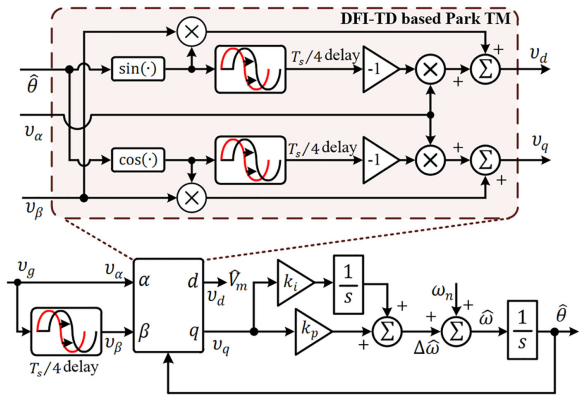

Fig. 5. Block diagram of truly NTD-PLL (tNTD-PLL).

also exhibits oscillatory errors. This is also confirmed using the numerical result as shown in Fig. 4, wherein a frequency jump of +3 Hz is provided to the NTD-PLL and its LTP model. The LTP model of NTD-PLL in Fig. 2 predicts the oscillatory behavior in $\hat{V}_m$ during frequency deviation but with some inaccuracies, due to linearization of the trigonometric terms [7]. However, the accuracy can further be increased when implementing the υ_d as well as υ_q using the actual trigonometric terms [6]. It is worth appreciating that, although the structure is referred to as NTD-PLL, the $\hat{V}_m$, $\hat{\omega}$, and $\hat{\theta}$ estimations obtained from NTD-PLL is still dependent on frequency deviation. On the other hand, the control loop of mNTD-PLL is free from DFOEs [6], but the $\hat{V}_m$ suffers from DFOE due to the presence of the DFOE term within the υ_d loop. Therefore, it is evident that the response

of mNTD-PLL is also dependent on frequency deviation. The elimination of the DFOE term from both the loops can be easily achieved by utilizing υ_d and υ_q of NTD-PLL and mNTD-PLL, respectively. To achieve this, the Park TM can be realized by using the first and second rows of (1) and (2), respectively, as

$$R_{dPT}\ \left(\hat{\theta}\right) = \begin{bmatrix} \cos\left(\hat{\theta} - \Delta\hat{\omega}\,(T_s/4)\right) & \sin\left(\hat{\theta}\right) \\ -\sin\left(\hat{\theta} - \Delta\hat{\omega}\,(T_s/4)\right) & \cos\left(\hat{\theta}\right) \end{bmatrix} \tag{3}$$

where R_{dPT} in (3) is referred to as DFOE immune (DFI) TD-based Park TM. This concept has been highlighted in Fig. 5 which results in the structure of tNTD-PLL. It is worth appreciating that under the frequency deviation, the first column elements of (3), as well as the quadrature-phase signal, υ_β obtained from the TD unit exhibit the same nonorthogonality under frequency, drift thus enabling elimination of DFOE from the $\hat{V}_m$ estimation in addition to elimination of DFOEs from $\hat{\omega}$ and $\hat{\theta}$ estimation.

A. LTP Modeling of tNTD-PLL

Let the in-phase signal, υ_α be expressed as

$$\upsilon_\alpha\ (t) = \upsilon_g\ \ (t) = V_m\ \ \cos(\omega_g t) = (V_n + \Delta V_m)\ \cos(\theta_g) \tag{4}$$

where υ_g is the grid voltage, and V_m and θ_g are the amplitude and phase angle of grid voltage, respectively. The term θ_g is defined as

$$\theta_g = \int \omega_g dt\ = \int (\omega_n + \Delta\omega_i)\, dt\ =\ \theta_n + \Delta\theta_g \tag{5}$$

where $\omega_g = \omega_n\ + \Delta\omega_i$ is the grid frequency with $\Delta\omega_i$ being frequency deviation from the nominal value (both in rad/s), respectively. The terms V_n, ω_n, and θ_n are the nominal voltage amplitude, frequency, and phase of the utility grid, while ΔV_m and $\Delta\theta_g$ are the amplitude and phase perturbation in the grid voltage waveform, respectively. The signal υ_β (i.e., the delay block output signal) under the frequency drift [2] is equal to

$$\begin{aligned} \upsilon_\beta\ (t) &= (V_m\,(t - T_s/4))\ \cos(\omega_g\,(t - T_s/4)) \\ &= (V_n + \Delta V_m\,(t - T_s/4)) \\ &\quad \times \cos(\theta_n - \pi/2 + \Delta\omega_i\,(t - T_s/4)) \\ &= \left(V_n + \Delta V_m^d\right)\ \sin\left(\theta_n + \Delta\theta_g^d\right) \end{aligned} \tag{6}$$

where $\Delta\, V_m^d = \Delta V_m(t - T_s/4)$ and $\Delta\,\theta_g^d = \Delta\theta_g(t - T_s/4)$. Using $\hat{\theta} = \theta_n\ + \Delta\hat{\theta}$ and $\Delta\ \hat{\theta}^d = \Delta\hat{\theta}(t - T_s/4)$ [7], the DFI TD-based Park transformation of tNTD-PLL in (3) can be rewritten as

$$\begin{bmatrix} \upsilon_d\,(t) \\ \upsilon_q\,(t) \end{bmatrix} = \begin{bmatrix} \cos\left(\theta_n + \Delta\hat{\theta}^d\right) & \sin\left(\theta_n + \Delta\hat{\theta}\right) \\ -\sin\left(\theta_n + \Delta\hat{\theta}^d\right) & \cos\left(\theta_n + \Delta\hat{\theta}\right) \end{bmatrix} \begin{bmatrix} \upsilon_\alpha\,(t) \\ \upsilon_\beta\,(t) \end{bmatrix}. \tag{7}$$

Using (4), (6) in (7), and solving for υ_d and υ_q gives (8) and (9), respectively, shown at the bottom of this page. Under the quasi-locked state, assuming $\Delta\hat{\theta} \approx \Delta\theta_g$, $\Delta\theta_g^d \approx \Delta\hat{\theta}^d$, and $\Delta V_m \approx \Delta\hat{V}_m$, and using trigonometric identities [7], (8) and (9) yields a set of LTP equations (10) and (11), respectively, shown at the bottom of this page. Using (10) and (11), the LTP model of the tNTD-PLL can be obtained as shown in Fig. 6. Based on the LTP model of tNTD-PLL, the following observations can be made.

1) Compared to NTD-PLL and mNTD-PLL, the DFOE term is neither coupled with υ_q nor with υ_d in tNTD-PLL. Therefore, the $\hat{\omega}$, $\hat{\theta}$, as well as $\hat{V}_m$ estimated from the tNTD-PLL structure will also be free from DFOEs and offset-errors during the grid frequency deviations. Since the responses of $\hat{V}_m$, $\hat{\omega}$, and $\hat{\theta}$ estimation is not dependent on grid frequency deviation; therefore, the structure is referred to as a tNTD-PLL.
2) The expression of υ_q of tNTD-PLL, as well as mNTD-PLL, is still the same. Thus, tNTD-PLL preserves the loop

$$\begin{aligned} \upsilon_d\ (t) &= (V_n + \Delta V_m)\ \cos(\theta_n + \Delta\theta_g)\cos\left(\theta_n + \Delta\hat{\theta}^d\right)\ + \left(V_n + \Delta V_m^d\right)\sin\left(\theta_n + \Delta\theta_g^d\right)\sin\left(\theta_n + \Delta\hat{\theta}\right) \\ &= (V_n + \Delta V_m)\,/2\ \left[\cos\left(\Delta\theta_g - \Delta\hat{\theta}^d\right) + \cos\left(2\theta_n + \Delta\theta_g + \Delta\hat{\theta}^d\right)\right] + \left(V_n + \Delta V_m^d\right)/2 \\ &\quad \times \left[\cos\left(\Delta\theta_g^d - \Delta\hat{\theta}\right) - \cos\left(2\theta_n + \Delta\theta_g^d + \Delta\hat{\theta}\right)\right] \end{aligned} \tag{8}$$

$$\begin{aligned} \upsilon_q\ (t) &= -\left(V_n + \Delta V_m\right)\cos(\theta_n + \Delta\theta_g)\sin\left(\theta_n + \Delta\hat{\theta}^d\right)\ + \left(V_n + \Delta V_m^d\right)\sin\left(\theta_n + \Delta\theta_g^d\right)\cos\left(\theta_n + \Delta\hat{\theta}\right) \\ &= (V_n + \Delta V_m)\,/2\ \left[\sin\left(\Delta\theta_g - \Delta\hat{\theta}^d\right) - \sin\left(2\theta_n + \Delta\theta_g + \Delta\hat{\theta}^d\right)\right] + \left(V_n + \Delta V_m^d\right)/2 \\ &\quad \times \left[\sin\left(\Delta\theta_g^d - \Delta\hat{\theta}\right) + \sin\left(2\theta_n + \Delta\theta_g^d + \Delta\hat{\theta}\right)\right] \end{aligned} \tag{9}$$

$$\upsilon_d\,(t) \approx V_n + \frac{1}{2}\left(\Delta V_m + \Delta V_m^d\right) + \frac{\cos(2\theta_n)}{2}\left(\Delta V_m - \Delta V_m^d\right) - \frac{V_n \sin(2\theta_n)}{2}\left[\left(\Delta\theta_g - \Delta\hat{\theta}\right) - \left(\Delta\theta_g^d - \Delta\hat{\theta}^d\right)\right] \tag{10}$$

$$\upsilon_q\,(t) \approx \frac{V_n}{2}\left[\left(\Delta\theta_g - \Delta\hat{\theta}\right) + \left(\Delta\theta_g^d - \Delta\hat{\theta}^d\right)\right] - \frac{\sin(2\theta_n)}{2}\left(\Delta V_m - \Delta V_m^d\right) - \frac{V_n \cos(2\theta_n)}{2}\left[\left(\Delta\theta_g - \Delta\hat{\theta}\right) - \left(\Delta\theta_g^d - \Delta\hat{\theta}^d\right)\right] \tag{11}$$

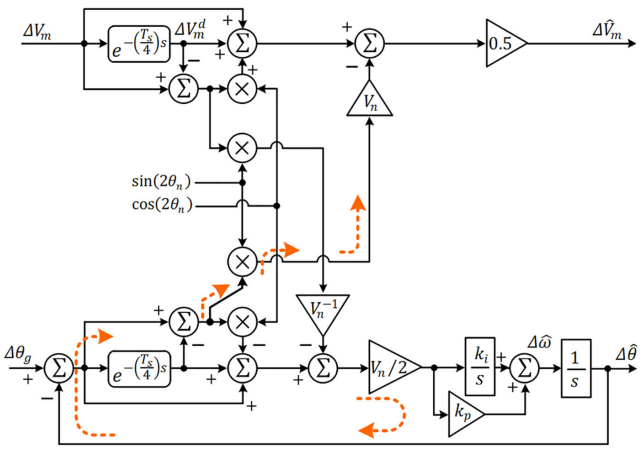

Fig. 6. LTP model of tNTD-PLL.

TABLE I
COMPUTATIONAL LOAD IN NTD-BASED PLLS AND THEIR PERFORMANCE COMPARISON: SAMPLING FREQUENCY = 10 kHz

	NTD-PLL	mNTD-PLL	tNTD-PLL
Stored Samples	100	100	150
Trigonometric functions	1	1	2
DFOR in $\hat{\theta}$	Poor	Perfect	Perfect
DFOR in $\hat{\omega}$	Poor	Perfect	Perfect
DFOR in $\hat{V}_m$	Good	Poor	Perfect

DFOR= Double-frequency oscillation rejection.

structure of mNTD-PLL as well as NTD-PLL and therefore, the existing tuning methodologies of NTD-PLL [2], [8] can be utilized for tuning the parameters of tNTD-PLL. Thus, using [2], the values for tNTD-PLL are obtained as $k_p = 166$ and $k_i = 11371$.

3) To highlight the significance of the proposed scheme, Table I summarizes the computational load of NTD-PLLs, i.e., the number of operations required for the quadrature signal generation and TM. Compared to NTD-PLL and mNTD-PLL, the tNTD-PLL exhibits only one additional fixed $T_s/4$ TD and trigonometric function.

B. Numerical Model Verification and Performance Comparison

The accuracy of the tNTD-PLL as well as its derived LTP models are evaluated under different grid disturbances through numerical studies in the MATLAB/Simulink. To that end, the procedure illustrated in [6] and [7] is utilized. Different grid disturbances like phase, frequency, and amplitude variations are applied to the LTP model of tNTD-PLL. The response of tNTD-PLL is finally compared with the prediction of its model. In the simulation study, the nominal grid amplitude and frequency of the grid and sampling frequency were taken as V_n= 325.27 V (= 1.0 p.u), 50 Hz, and 10 kHz, respectively. Fig. 7 illustrates the numerical results. The following key observations can be made.

1) The LTP model of tNTD-PLL accurately predicts the dynamics of estimation parameters, i.e., $\hat{V}_m$, $\hat{\omega}$, and $\hat{\theta}$ under phase, frequency, as well as amplitude variations.
2) It is worth appreciating from Fig. 7(d) that the estimation of grid parameters from suggested tNTD-PLL is free from DFOEs during the frequency deviation.
3) Due to the same loop structure of tNTD-PLL and NTD-PLL, the tNTD-PLL also suffers from the distorted response during dc offset and harmonic disturbances, similar to the NTD-PLL [2], [8], [9].
4) The derived LTP model neglects the presence of dc offset and harmonic disturbances in the grid. Therefore, the LTP model does not predict the oscillatory response in the estimations of $\hat{V}_m$, $\hat{\omega}$, and $\hat{\theta}$ during dc offset and harmonic disturbances.

III. PERFORMANCE EVALUATION

The performance of the tNTD-PLL is evaluated and compared with the NTD-PLL [2], mNTD-PLL [6], and frequency-fixed second-order generalized integrator-based PLL (FFSOGI-PLL) [4], [10] through extensive experimental studies using the dSPACE DS1104 hardware [4], [6], [8]. The control parameters of the NTD-PLL, as well as mNTD-PLL, are set as $k_p = 166$ and $k_i = 11371$ since the studied NTD-based PLLs exhibits the same loop structure [2], [6], whereas the parameters of FFSOGI-PLL are set as $k_p = 137.50$ and $k_i = 7878$ [4], [10]. Fig. 8 shows the experimental results of parameters estimation obtained using the explored PLLs under different grid disturbances. Throughout the result plots, each column represents different grid disturbances while the first row of the subplots show amplitude estimation, $\hat{V}_m$ in (V), second row gives frequency estimation, $\hat{f} = \hat{\omega}/2\pi$ in (Hz) while third row corresponds to phase error estimations, $\Delta\theta = \theta_g - \hat{\theta}$ in (°), respectively. Fig. 8(a) shows the result during the start-up of the PLLs. Except for tNTD-PLL and mNTD-PLL, the FFSOGI-PLL and NTD-PLL show poor estimation responses during the starting of the PLLs operation. All the PLLs shows bounded responses in the estimation of $\hat{V}_m$, $\hat{\omega}$, and $\hat{\theta}$ during phase jump and amplitude disturbances as shown in Fig. 8(b) and (c), respectively.

Fig. 8(d) shows that during frequency jump, the FFSOGI-PLL shows DFOEs in $\hat{V}_m$, $\hat{\omega}$, and $\hat{\theta}$, along with offset error in $\hat{\theta}$. The NTD-PLL do not have offset error issues, but, it exhibits DFOEs in $\hat{\omega}$ and $\hat{\theta}$. Moreover, due to cross-coupling between amplitude and phase estimation loops as discussed in Section II, the NTD-PLL also exhibits oscillations in $\hat{V}_m$. Although the $\hat{\omega}$ and $\hat{\theta}$ estimated from mNTD-PLL are free from DFOEs and offset errors, but $\hat{V}_m$ suffers from a DFOE [6]. However, contrary to NTD-PLL, mNTD-PLL, and FFSOGI-PLL which suffers from a combination of offset error and DFOEs in one or more estimation parameters during the frequency deviation, the estimated parameters viz-a-viz $\hat{V}_m$, $\hat{\omega}$, and $\hat{\theta}$ obtained from tNTD-PLL are free from such errors and shows a better transient and steady-state response. Fig. 8(e) shows the performance of the PLLs when the grid is restored to nominal condition. Thus, the results shown in Fig. 8 highlight the promising performance

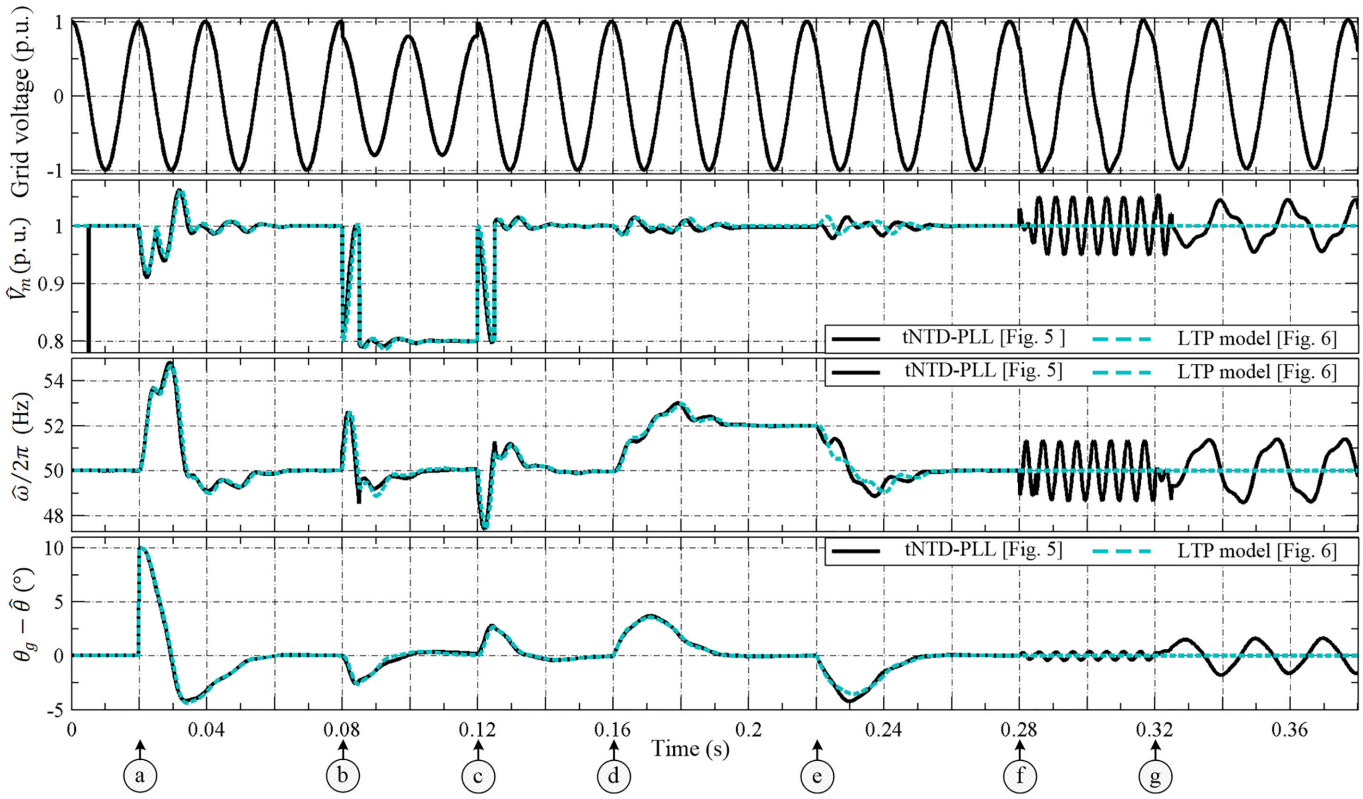

Fig. 7. Numerical model verification under (a) 10° Phase jump, (b) 0.2 p.u. Sag, (c) nominal amplitude restored, (d) +2 Hz frequency jump, (e) nominal frequency restored, (f) 0.05 p.u. fifth harmonic, and (g) 0.02 p.u. dc offset.

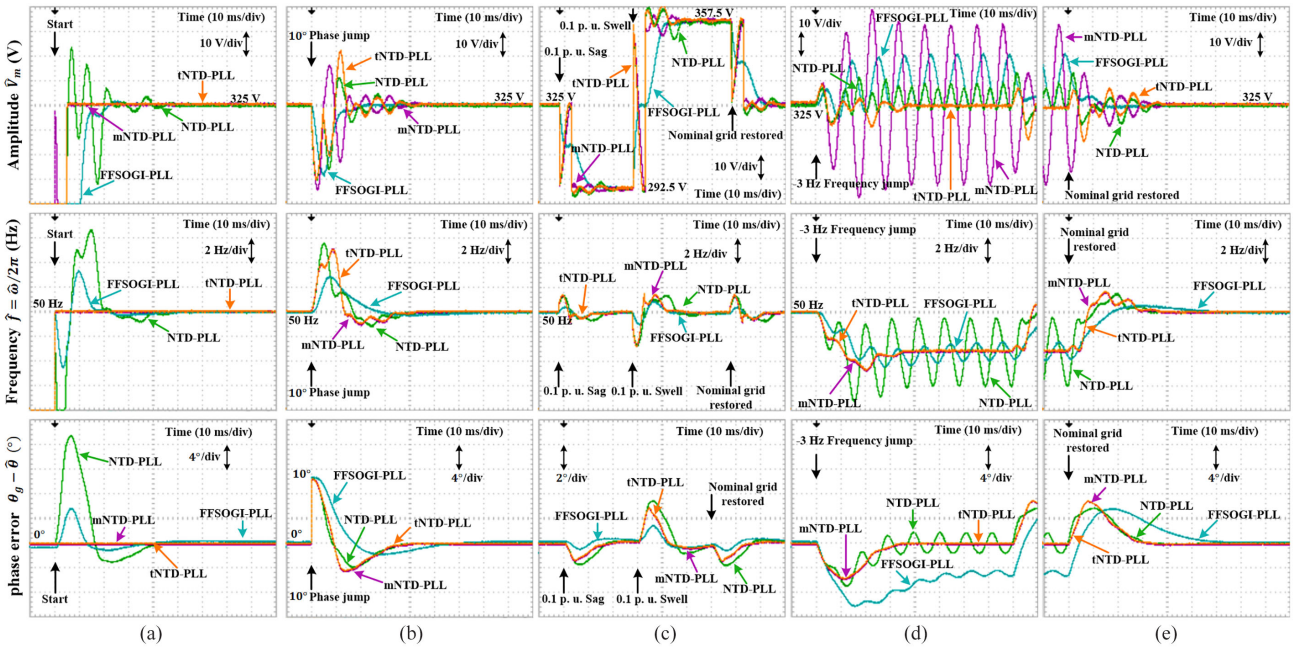

Fig. 8. Experimental results of the performance of PLLs. (a) During the start. (b) 10° phase jump. (c) 0.1 p.u. Sag and 0.1 p.u. swell. (d) −3 Hz frequency jump. (e) Nominal grid restored.

of the proposed tNTD-PLL over NTD-PLL, mNTD-PLL, and FFSOGI-PLL under the studied disturbances.

IV. Conclusion

In this letter, it has been shown that the dynamic response of standard NTD-PLL under the frequency deviation can be improved by including an additional TD unit and trigonometric function in Park TM, the structure of which was named tNTD-PLL. The LTP model of the tNTD-PLL was obtained to verify the stability of the proposed technique. The effectiveness of the suggested strategy was finally confirmed using the numerical and experimental results.

References

[1] S. Golestan, J. M. Guerrero, and J. C. Vasquez, "Single-Phase PLLs: A review of recent advances," *IEEE Trans. Power Electron.*, vol. 32, no. 12, pp. 9013–9030, Dec. 2017.

[2] S. Golestan, J. M. Guerrero, A. Vidal, A. G. Yepes, J. Doval-Gandoy, and F. D. Freijedo, "Small-Signal modeling, stability analysis and design optimization of single-phase delay-based PLLs," *IEEE Trans. Power Electron.*, vol. 31, no. 5, pp. 3517–3527, May 2016.

[3] M. A. Akhtar and S. Saha, "Analysis and comparative studies on impact of transport delay and transforms on the performance of TD-PLL for single phase GCI under grid disturbances," *Int. J. Elect. Power Energy Syst.*, vol. 115, Feb. 2020, Art. no. 105488.

[4] M. A. Akhtar and S. Saha, "An adaptive frequency-fixed second-order generalized integrator-quadrature signal generator using fractional-order conformal mapping based approach," *IEEE Trans. Power Electron.*, vol. 35, no. 6, pp. 5548–5552, Jun. 2020.

[5] S. Golestan, J. M. Guerrero, J. C. Vasquez, A. M. Abusorrah, and Y. Al-Turki, "All-pass-filter-based PLL systems: Linear modeling analysis and comparative evaluation," *IEEE Trans. Power Electron.*, vol. 35, no. 4, pp. 3558–3572, Apr. 2020.

[6] M. A. Akhtar, S. Saha, and R. Singh, "A second look on nonfrequency-dependent transport delay-based PLL: Performance enhancement under frequency deviations," *IEEE Trans. Power Electron.*, vol. 36, no. 12, pp. 13365–13371, Dec. 2021.

[7] S. Golestan, J. M. Guerrero, and J. C. Vasquez, "LTP modeling of single-phase T/4 delay-based PLLs," *IEEE Trans. Ind. Electron.*, vol. 68, no. 9, pp. 9003–9008, Sep. 2021.

[8] M. A. Akhtar and S. Saha, "A systematic approach of loop filter tuning of TD-based PLLs using LQR based approach considering time-delay," *IEEE J. Emerg. Sel. Topics Power Electron.*, Early Access, doi: 10.1109/JESTPE.2020.3043490.

[9] S. Golestan, J. M. Guerrero, A. Abusorrah, M. M. Al-Hindawi, and Y. Al-Turki, "An adaptive quadrature signal generation-based single-phase phase-locked loop for grid-connected applications," *IEEE Trans. Ind. Electron.*, vol. 64, no. 4, pp. 2848–2854, Apr. 2017.

[10] F. Xiao, L. Dong, L. Li, and X. Liao, "A frequency-fixed SOGI-based PLL for single-phase grid-connected converters," *IEEE Trans. Power Electron.*, vol. 32, no. 3, pp. 1713–1719, Mar. 2017.